ACS Sustainable Chemistry & Engineering

Research Article

Cite This: ACS Sustainable Chem. Eng. 2019, 7, 16041−16049

pubs.acs.org/journal/ascecg

# Investigating New Routes for Biomass Upgrading: "$H_2$-Free" Hydrodeoxygenation Using Ni-Based Catalysts

W. Jin,[†] L. Pastor-Pérez,[†,‡] Juan J. Villora-Picó,[‡] A. Sepúlveda-Escribano,[‡] S. Gu,[†] and T. R. Reina*[,†]

[†]Department of Chemical and Process Engineering, University of Surrey, Guildford GU2 7XH, U.K.

[‡]Laboratorio de Materiales Avanzados, Departamento de Química Inorgánica—Instituto Universitario de Materiales de Alicante, Universidad de Alicante, Alicante E-03080, Spain

Supporting Information

**ABSTRACT:** This work showcases an innovative route for biocompound upgrading via hydrodeoxygenation (HDO) reactions, eliminating the need for external high-pressure hydrogen supply. We propose the use of water as reaction media and the utilization of multifunctional catalysts that are able to conduct multiple steps such as water activation and HDO. In this study, we validate our hypothesis in a high-pressure batch reactor process using guaiacol as a model compound and multicomponent Ni-based catalysts. In particular, a comparison between ceria-supported and carbon/ceria-supported samples is established, the carbon-based materials being the suitable choice for this reaction. The physicochemical study by X-ray photoelectron spectroscopy, transmission electron microscopy, X-ray diffraction, and temperature-programmed reduction reveals the greater dispersion of Ni clusters and the strong metal-support interaction in the carbon/ceria-based samples accounting for the enhanced performance. In addition, the characterization of the spent samples points out the resistance of our catalysts toward sintering and coking. Overall, the novel catalytic approach proposed in this paper opens new research possibilities to achieve low-cost bio-oil upgrading processes.

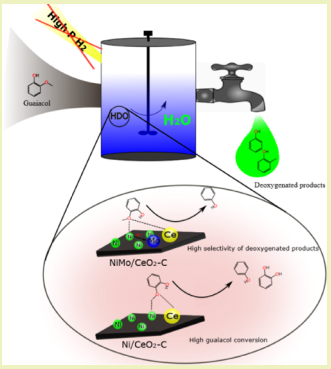


**KEYWORDS:** *biomass upgrading, hydrodeoxygenation, water activation, nickel, carbon/ceria-based catalysts*

## INTRODUCTION

The rapid depletion of fossil fuel encourages energy research towards seeking environmentally friendly and sustainable resources to satisfy the increasing energy demand.[1] Biomass feedstocks are promising candidates which own multiple advantages such as their abundance, local availability, renewable character, and so forth.[2,3] Bio-oil derived from pyrolysis processes has the potential to be used as liquid fuel or to be further upgraded into added-value chemicals. However, high oxygen content (up to 47 wt %)[4] leads to an adverse effect on the chemical and physical properties of bio-oil, such as low energy density, high corrosivity, thermal and chemical instability, and so forth, compared to conventional fossil fuels.[5,6] In order to address these problems, catalytic hydrodeoxygenation (HDO) technology was proposed as a standard route to effectively conduct bio-oil upgrading. Typically, in this process, oxygen is removed in the form of water with the participation of high-pressure $H_2$ (eq 1).[7]

$$R - OH + H_2 \rightarrow R - H + H_2O \quad (1)$$

The HDO process is typically carried out at relatively low reaction temperatures (200−400 °C) and high hydrogen pressure (4−20 MPa)[8] in batch or fixed-bed reactors. In this sense, the widespread implementation of HDO is limited by the supply of high-pressure $H_2$. On the one hand, commercial $H_2$, typically produced from steam reforming of fossil fuels (natural gas, oil, and coal)[9] or water electrolysis,[10] is an expensive energy resource. On the other hand, $H_2$ as a reactant presents some inherent hazards in terms of transportation, storage, and operation when it mixes with air within a wide range of concentrations (4−75.6% v/v).[11] In order to overcome these limitations, the development of novel approaches, where the supply of external $H_2$ can be suppressed, has attracted the interest of the catalysis community.

To date, several methods (e.g., catalytic transfer hydrogenation (CTH), reforming followed by HDO, the combination of metal oxidation with water and HDO, nonthermal plasma (NTP) technology[12]) have been proposed to realize the deoxygenation reaction with in situ hydrogen generation. In the CTH process, first, hydrogen is produced from the dehydrogenation of an hydrogen donor solvent (e.g., formic acid).[13] The HDO process can subsequently take place with the generated hydrogen through a metal hydride route.[14] Generally, the CTH method is favorable for effective partial deoxygenation of phenolics. However, the disposition of byproducts produced from dehydrogenation of a hydrogen donor cannot be ignored. Moreover, the undesired side reactions (such as dehydration) will pose an adverse effect on the catalyst. In contrast, the tandem reforming (e.g., methane or alcohols)[15,16] followed by HDO is more

Received: May 14, 2019
Revised: July 24, 2019
Published: August 28, 2019

competitive considering its high efficiency for total deoxygenation. For instance, Lee et al.[17,18] developed a novel MgNiMo/activated charcoal (AC) catalyst and used it in the catalytic upgrading of biotar under supercritical ethanol conditions. More than 70.1 wt % of high-yield liquid and little coke was produced from pyrolytic oil over MgNiMo/AC.[18] It is noteworthy that metal oxidation with $H_2O$ (i.e., Zn) followed by subsequent HDO is an attractive approach because cheap water is used as the hydrogen source. Nevertheless, the regeneration of metal requires a high energy input,[19,20] limiting its industrial application. NTP technology is overshadowed compared to the other three strategies because of the low selectivity of deoxygenated products, although it has the advantage of fairly mild reaction conditions.[21,22] Overall, novel methods with economic advantages and high deoxygenation efficiency for in situ HDO are still under intensive explorations.

Undoubtedly, it is ideal to use water as the hydrogen source during the in situ HDO process, considering that it is readily available and the economic advantages of water over other candidates. Accordingly, we propose a novel HDO method to conduct HDO suppressing external $H_2$ supply, thus improving remarkably the economic viability and the safety aspects in comparison with traditional HDO pathways. It is envisioned that water would undergo a splitting process on the catalytic surface to produce hydrogen. Hence, hydrogen can further participate in the HDO of bio-oil, facilitating the C−O bond breaking and ultimately the oxygen removal from the organic molecules. Certainly, our hypothesis is an ambitious approach that requires multifunctional catalysts able to: (i) conduct the water splitting in the selected reaction conditions and (ii) catalyze the HDO process using the in situ produced hydrogen.

A rational catalyst design is needed to tackle this challenge. Our group has recently proposed the implementation of lessons learnt from traditional HDO to design novel materials for "$H_2$-free" HDO reactions.[12] For example, Ni-based catalysts have been proven to be effective candidates for HDO reactions.[23] Moreover, the combination of Ni with another oxyphilic metal (i.e., Mo) can achieve the HDO with high oxygen-removal efficiency to produce aromatic compounds.[24] Besides, cerium oxide is a promising catalyst support and promoter for this reaction because of its high oxygen storage capacity and suitability to activate oxygen-containing molecules.[25] Potentially, $CeO_2$ could provide oxygen adsorption sites and facilitate hydrogen release from water. Activated carbon possesses extraordinarily high surface area and hence is widely used as adsorbent material. Additionally, activated carbon is also a viable support considering its hydrophobicity, which could decrease the possibility of metal deactivation in water-existing reaction systems.[26] The adsorption of water on the catalysts' surface is necessary to achieve hydrogen production, but too much water would block the active sites of the catalyst and would inevitably decrease the encounter possibilities between the reactant and catalyst. Hence, a tradeoff has to be reached to balance the adsorption of water and reactants on the surface of the catalyst. In this sense, the polarity of the support has a huge impact on the process.

Under these premises, in our work, a series of Ni-based catalysts supported on $CeO_2$ with/without activated carbon (C) have been synthesized, characterized, and studied for the guaiacol HDO in a high-pressure batch reactor. In this process, the effect of support species and the addition of Mo as a promoter were investigated. This novel approach may have a strong impact on the way we conceive HDO reactions and could open new avenues for research in the development of bio-oil upgrading processes.

## MATERIALS AND METHODS

**Materials.** Chemicals used for catalysts synthesis, that is, nickel nitrite hexahydrate ($Ni(NO_3)_2{\cdot}6H_2O$), molybdate tetrahydrate ($(NH_4)_6Mo_7O_{24}{\cdot}4H_2O$), cerium nitrate hexahydrate ($Ce(NO_3)_3{\cdot}6H_2O$), and urea ($CH_4N_2O$) were all supplied by Sigma-Aldrich Co., Ltd. Activated carbon (RGC 30) was provided by Westvaco. Guaiacol, solvents (ethyl acetate and acetone), and chemicals used for calibration (including phenol, *o*-cresol and catechol) were also supplied by Sigma-Aldrich Co., Ltd.

**Methods.** *Catalyst Preparation.* Detailed information of the catalysts synthesis can be found in the Supporting Information. Briefly, we have two series of samples containing 15 wt % of Ni supported on $CeO_2$ or activated carbon, and 2 wt % of Mo as a promoter was considered in both series. The carbon-based family was also promoted with 10 wt % of $CeO_2$.

*Catalyst Characterization.* The catalysts have been carefully characterized by means of X-ray diffraction (XRD), Raman, transmission electron microscopy (TEM), X-ray photoelectron spectroscopy (XPS), and $N_2$-adsorption. When appropriate, fresh/spent samples have been analyzed. Full description of the characterization techniques is given in the electronic Supporting Information.

*Catalytic Reactions.* The HDO reactions were conducted in a high-pressure batch reactor (Parr Series 5500 HPCL Reactor with a 4848 Reactor Controller) using poly(tetrafluoroethylene) gaskets at 250 °C and 50 bar 1 wt % of guaiacol in water (0.5 g guaiacol), and 0.2 g of the catalyst was loaded in a glass-lined steel vessel. Full details of the reaction setup and products analysis are described in the Supporting Information.

## RESULTS AND DISCUSSION

**Characterization of the Calcined Catalysts.** *$H_2$-TPR.* Redox properties and information concerning metal-support interactions were studied by $H_2$-temperature-programmed reduction (TPR) analysis. Figure 1 shows the $H_2$-TPR profiles of all calcined catalysts. Different reduction zones can be observed in the TPR profile of $Ni/CeO_2$. Two small peaks at low temperature (around 211 and 255 °C) correspond to the reduction of finely dispersed NiO on the support. Ceria is also a reducible material, and indeed, it is reported that the

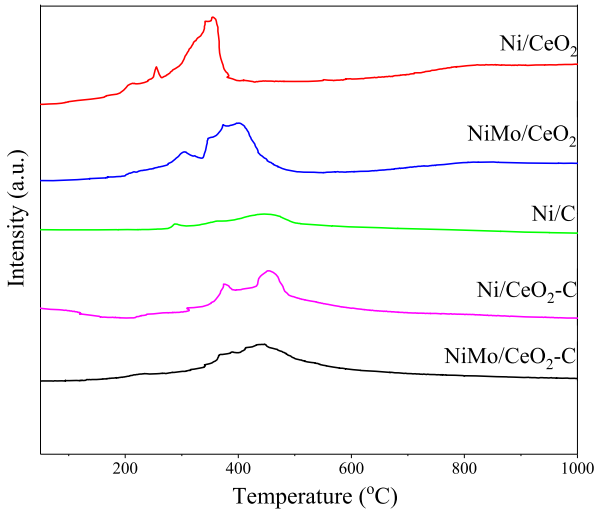


**Figure 1.** $H_2$-TPR profiles of studied catalysts.



DOI: 10.1021/acssuschemeng.9b02712
ACS Sustainable Chem. Eng. 2019, 7, 16041−16049

reduction temperature of ceria can be decreased in the presence of Ni due to hydrogen spillover.[28] In fact, the intermediate reduction zone observed in this sample (around 353 °C) can be ascribed to the reduction of medium-sized Ni particles along with ceria surface reduction indicating a certain degree of Ni−Ce interaction. The small and broad zone at high temperature (around 800 °C) can be assigned to the reduction of bulk $CeO_2$, as previously reported elsewhere.[29]

As for the bimetallic Ni−Mo/$CeO_2$ catalysts, the TPR profile is in general terms very similar to that of the Ni/$CeO_2$ but with a shift of the medium-temperature reduction processes toward higher temperatures. It is reported that the typical reduction step of molybdenum trioxide ($Mo^{6+} \rightarrow Mo^{4+}$) in amorphous, multilayered Mo oxides or octahedral Mo species should be presented at temperatures around 544 °C.[30] However, no apparent reduction zone can be observed around 544 °C in the TPR profile of NiMo/$CeO_2$. Perhaps the lack of Mo reduction peaks is due to the low Mo loading (2 wt %) in the NiMo/$CeO_2$ catalysts and/or the observed shift of the reduction zones accounts for interaction among Mo−Ni−Ce particles. The main reduction zone of NiMo/$CeO_2$ is centered at a temperature around 398 °C, which is higher than that of Ni/$CeO_2$ (357 °C) and lower than that of $MoO_3$ (544 °C). A similar delay on the reducibility of Ni−Mo materials compared to monometallic Ni materials was observed in Myint's study and was attributed to the metal−metal interaction.[31]

Regarding the TPR profiles of C-containing catalysts, two reduction zones can be observed for the Ni/C catalyst. Similar to the ones of $CeO_2$-supported catalysts, the first reduction zone at low temperature (287 °C) is ascribed to the reduction of highly dispersed NiO, while the wide ranged peak at intermediate temperature (450 °C) can be attributed to the reduction of medium-sized Ni particles. In contrast, three apparent reduction zones (318, 380, and 455 °C) were exhibited for the Ni/$CeO_2$−C catalyst. Again, the first reduction zone is attributed to the reduction of highly dispersed NiO on the support, and the middle two peaks at intermediate temperatures correspond to the dual effect of the reduction of medium-sized Ni particle and surface reduction of ceria with interaction with nickel. Interestingly, the addition of Mo to the C-based sample makes the overall reduction process more homogeneous. The homogenization of the TPR profiles has been previously reported for multicomponent catalysts, and it is a consequence of the multiple electronic interactions among the different high dispersed species due to the use of a high surface support (in this case, Mo, Ni, $CeO_2$, and C), resulting in the overlapping of the expected reduction events (NiO, $CeO_2$, and $MoO_x$ reduction). In any case, it is worth to emphasize the enhanced interaction among the different species observed in the C-based multicomponent material, NiMo/$CeO_2$−C, and its potential impact on the catalytic activity.

*X-ray Diffraction.* XRD patterns of calcined support and catalysts are shown in Figure 2. The characteristic $CeO_2$ peaks (JCPDS 34-0394) at 28.6°, 33.4°, 47.8°, and 56.7° can be clearly observed in the XRD patterns of $CeO_2$- and $CeO_2$−C-supported catalysts, corresponding to the reflections in (111), (200), (220), and (331) crystalline planes of the cubic fluorite-type phase, respectively. For the C-free samples, the sharp diffraction peaks of $CeO_2$ indicate a high degree of crystallinity and relatively higher crystal size. In contrast, the $CeO_2$ diffraction peaks for the C-containing catalysts are much

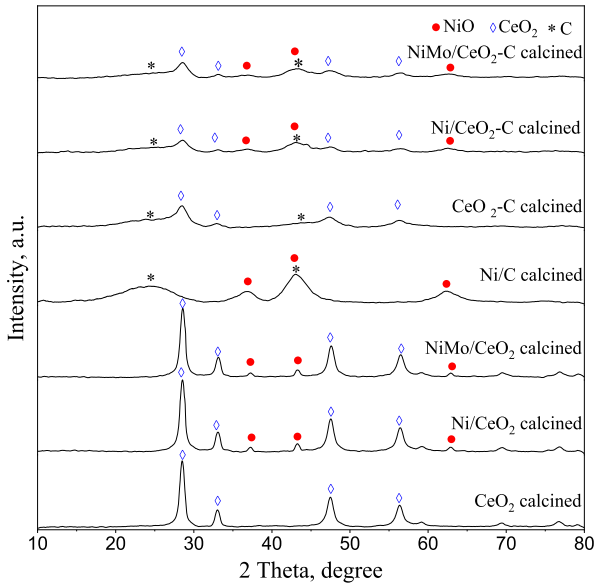


**Figure 2.** XRD patterns of calcined catalysts.

wider, indicating small crystal size and greater ceria dispersion. Hence, a larger exposed surface is expected for these materials (higher surface to volume ratio) compared to the $CeO_2$ bulk-supported catalysts. The diffraction peaks at 37.2°, 43.3°, and 62.9° correspond to the (111), (200), and (220) planes, respectively, of NiO face-centered-cubic phase (JCPDS 04-0835). Once again, the broader diffraction peaks of NiO in C-containing catalysts reveal a small crystal size and a higher dispersion of Ni particles in comparison to the C-free materials. Crystalline Mo species were not detected in any of the studied samples. The absence of Mo species in XRD patterns could be attributed to the low metal loading of Mo (2 wt %), its good dispersion amorphous character and/or the overlapping of $MoO_x$ reflections with diffraction peaks of $CeO_2$.

The XRD patterns in Figure 2 just confirm the successful preparation of the studied catalysts and the superior metallic dispersion achieved when using activated carbon as support. However, the samples were pretreated in hydrogen prior to the reaction. The XRD patterns of the activated catalysts are shown in Figure S1. Diffraction peaks belonging to metallic Ni nanoparticles (JCPDS 87-0712)[32,33] are now clearly observed. The wide peaks of metallic Ni presented in C-containing catalysts indicate small particle size and high dispersion of Ni crystallites on the support. Metallic Ni reflections are more marked in the XRD pattern of the C-free materials, showing both NiMo/$CeO_2$ and Ni/$CeO_2$, a very similar pattern.

*$N_2$ Adsorption Isotherms.* Table 1 shows the specific surface area ($S_{BET}$), the micropore volume ($V_{micro}$, D−R), and the total pore volume ($V_{total}$) for all calcined catalysts. Activated carbon has the largest surface area ($S_{BET}$ = 1487 $m^2/g$) and pore volume ($V_{micro}$ = 0.52 $cm^3/g$; $V_{total}$ = 1.14 $cm^3/g$). The larger surface area ($S_{BET}$), $V_{micro}$, and $V_{total}$ of the $CeO_2$−C-containing catalysts compared to that of $CeO_2$-supported catalysts can be attributed to the superior textural properties of activated carbon. The addition of $CeO_2$ to Ni/C formulation slightly decreased the surface area of Ni/C in good agreement with previous observations in the literature.[25,34] The slight depletion of the surface area is attributed to the larger mass and lower porosity of ceria as compared to carbon.[24] The


DOI: 10.1021/acssuschemeng.9b02712
ACS Sustainable Chem. Eng. 2019, 7, 16041−16049

**Table 1. Textural Properties of Supports and Catalysts**

| | $S_{BET}$ ($m^2/g$) | $V_{micro}$ ($cm^3/g$)[a] | $V_{total}$ ($cm^3/g$) |
|---|---|---|---|
| $CeO_2$[25] | 101 | 0.04 | 0.11 |
| $Ni/CeO_2$ | 78 | 0.029 | 0.064 |
| $NiMo/CeO_2$ | 46 | 0.017 | 0.069 |
| AC[25] | 1487 | 0.52 | 1.14 |
| Ni/C | 1062 | 0.378 | 0.85 |
| $Ni/CeO_2$−C | 1027 | 0.368 | 0.79 |
| $NiMo/CeO_2$−C | 1017 | 0.364 | 0.79 |

[a]Micropore volumes are calculated by the DR method.

specific surface area and $V_{micro}$ decreased slightly, whereas the $V_{total}$ remains stable upon the addition of Mo in the catalyst formula which indicated that Mo has a minor impact on the catalyst's textural properties probably because of the low amount of Mo used in the preparation.

*Transmission Electron Microscopy.* Figure 3 shows the TEM images of all calcined catalysts. The micrographs show

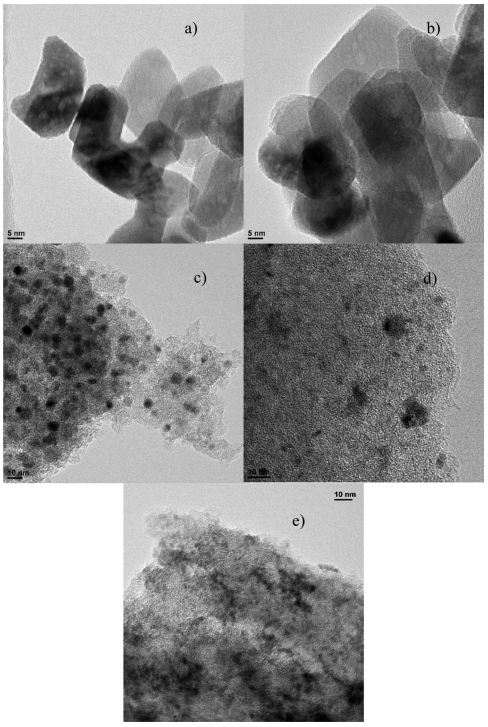


**Figure 3.** TEM micrographs of calcined catalysts. (a) $Ni/CeO_2$; (b) $NiMo/CeO_2$; (c) Ni/C; (d) $Ni/CeO_2$−C; (e) $NiMo/CeO_2$−C.

the relatively large crystal sizes of $CeO_2$ and NiO in $Ni/CeO_2$ and $NiMo/CeO_2$ catalysts in fair agreement with the XRD data. In comparison, active phases are homogeneously dispersed on the C-based support, with no big agglomerations being observed. The addition of $CeO_2$ enhanced the Ni dispersion in the carbon-containing catalysts, as can be seen from the larger particle size of NiO in Ni/C compared to $CeO_2$−C supported catalysts. The smaller particle size of NiO and $CeO_2$ observed in the C-supported catalyst compared to bulk $CeO_2$-supported catalysts confirmed the XRD results. It has to be pointed out that it is difficult to distinguish among $CeO_2$, NiO, and $MoO_3$ in the TEM images due to their similar electron density because they all appear as dark dots in the images.[25] Hence, the particle size distribution was only estimated for the Ni/C sample (Figure S2), showcasing a mean particle size of 5.1 ± 1 nm in good agreement with the XRD results. In any case, from the combined TEM and XRD analysis, we can conclude that the $CeO_2$−C-supported samples are composed of small nanoclusters of NiO/Ni−$CeO_2$ crystals doped with $MoO_x$ very well dispersed in the activated carbon matrix, and clearly, the active phases are much better dispersed in the carbon-based materials than in the bulk ceria-supported samples.

*X-ray Photoelectron Spectroscopy.* The oxidation state and the chemical environment on the surface of the reduced catalysts were investigated by XPS. XPS spectra of Ni $2p_{3/2}$ and Mo $3d_{5/2}$ are given in Figures S3 and S4, respectively. Further information regarding the binding energies (B.E.) of the main peaks of Ni $2p_{3/2}$ and Mo $3d_{5/2}$, the different metal/oxide ratios, and the $Ce^{3+}$ % are summarized in Table 2.

It seems clear that different nickel species exist on the surface of catalysts as intended from the complex Ni $2p_{3/2}$ spectra (Figure S3). The first band with low B.E. at around 852−853 eV is assigned to metallic nickel species. The following two bands (854−857 eV) can be assigned to $Ni^{2+}$ species with different chemical environments.[35,36]

For bulk ceria-supported catalysts, the Ni species in $Ni/CeO_2$ are more electronically charged (lower B.E.) than the Ni species in the $NiMo/CeO_2$ system. The addition of Mo shifted the B.E. of Ni species into higher values, verifying the close contact among Ni−Mo−Ce. Indeed, the existence of a Ni−Mo and strong metal-support interactions can modify the structure and electronic properties of Ni, which is fundamental for reactant activation and hence remarkably influences the catalytic behavior of this system.[37] However, for this bulk ceria-supported sample, the Ni−Mo−Ce interaction does not contribute as much as in the C-supported sample to the homogeneity of the peak which can be seen in TPR profiles (Figure 1), and it will be discussed evidencing the connection among TPR and XPS data.

As for the C-containing catalysts, the addition of $CeO_2$ into the Ni/C slightly shifts the Ni species to higher B.E. It is worth to point out that further addition of Mo in the $Ni/CeO_2$−C catalyst results in an increase of the Ni−Ce−Mo interactions,

**Table 2. B.E. of Ni $2p_{3/2}$ and Mo $3d_{5/2}$ Levels and Ratios of Species of Reduced Catalysts**

| | Ni $2p_{3/2}$ | | | Mo $3d_{5/2}$ | | | Ce 3d |
|---|---|---|---|---|---|---|---|
| | $Ni^0$ | $Ni^{2+}$ | $Ni^0/Ni^{2+}$ | $Mo^{5+}$ | $Mo^{6+}$ | $Mo^{5+}/Mo^{6+}$ | $Ce^{3+}$ |
| catalysts | B.E. (eV) | B.E. (eV) | at/at | B.E. (eV) | B.E. (eV) | at/at | % |
| $Ni/CeO_2$ | 852.10 | 854.14−856.64 | 0.61 | | | | 32 |
| $NiMo/CeO_2$ | 852.55 | 854.40−856.66 | 0.47 | | 232.55 | | 32 |
| Ni/C | 852.87 | 853.73−856.21 | 0.47 | | | | |
| $Ni/CeO_2$−C | 852.99 | 854.05−856.04 | 0.50 | | | | 40 |
| $NiMo/CeO_2$−C | 853.11 | 854.82−856.60 | 0.79 | 230.78 | 232.88 | 1.09 | 43 |



DOI: 10.1021/acssuschemeng.9b02712
ACS Sustainable Chem. Eng. 2019, 7, 16041−16049

considering that the peak is further displaced to higher B.E. In addition, for this NiMo/$CeO_2$−C sample, the $Ni^0/Ni^{2+}$ ratio increased significantly, indicating greater availability of the Ni active phase in this sample. The shifting phenomenon to higher B.E. values of Ni species in the case of C-containing catalysts reveals the higher positive character of the Ni species in these samples. Such a situation provided a good deal of preferential sites for the anchoring and cleavage of the electronically charged oxygen atoms coming from water or the organic biocompound.

Concerning the Mo oxidation state, a sole band in the Mo $3d_{5/2}$ region for the NiMo/$CeO_2$ catalyst reveals the presence of only $Mo^{6+}$. Interestingly, both $Mo^{5+}$ and $Mo^{6+}$ species[38] exist on the surface of the NiMo/$CeO_2$−C catalyst. This result indicates that the activated carbon helps to stabilize the multiple Mo oxidation states together with the Ni−Mo−Ce-support electronic interaction that helps $Mo^{6+}$ to be reduced to $Mo^{5+}$. Also, the observed Mo reduction may account for the higher B.E. achieved for Ni species in this sample, pointing an electronic transfer Ni−Mo.

As for the Ce 3d XPS results, the complexity of spectra (not shown) indicates the coexistence of $Ce^{4+}$ and $Ce^{3+}$ species in the catalysts, which confirms the existence of the $Ce^{4+}/Ce^{3+}$ redox pair responsible for the versatile redox properties of ceria-containing materials.[39] One of the key aspects in catalysis by ceria and ceria-doped materials is the population of oxygen vacancies, given their role in multiple reactions. Although an accurate estimation of such punctual defects is beyond the scope of this study, it is well-accepted that oxygen defects in ceria are associated to $Ce^{3+}$. Therefore, the percentage of $Ce^{3+}$ provides a rough idea of the relative oxygen vacancy concentration. As shown in Table 2, the use of activated carbon as support increased the percentage of $Ce^{3+}$ in these samples, indicating a greater population of oxygen defects on the surface in C-containing catalysts which certainly helps to overcome water activation.[35] In addition, as previously reported, oxygen vacancies are envisaged as preferential sites for metallic particle nucleation increasing the metallic dispersion, which reinforces the results obtained by TEM and XRD.[40,41] Very interestingly, the percentage of $Ce^{3+}$ increases with the addition of well-dispersed Mo in the carbon-based catalysts, pointing out the important role of Mo and C to facilitate the reduction of $Ce^{4+}/Ce^{3+}$ and hence create defects sites for reactant activation.

**Catalytic Activity.** The catalytic performance of the studied catalysts in the guaiacol HDO process without the supply of external $H_2$ is presented in Figures 4 and S5. The guaiacol conversion (eq 1) over different catalysts is presented in Figure 4. Clearly, $CeO_2$−C-supported catalysts are more active than $CeO_2$-supported catalysts in terms of guaiacol conversion. It has to be highlighted that the carbon-free solids show similar conversions to the blank run, but with the Mo-containing sample improving the overall selectivity. For this sample, the majority of the products were partial deoxygenated compounds, indicating the key role of Mo to tune selectivity toward desired products. Herein, we have to emphasize the remarkable difficulty of the reaction we are trying to achieve, that is, HDO suppressing the supply of external hydrogen and using water as a hydrogen donor. On the other hand, the fact that the carbon-based materials displayed conversions close to or even over 20% is a big achievement and a step forward to explore the viability of this completely new route. Slightly higher guaiacol conversion, 22%, was obtained over a Ni/

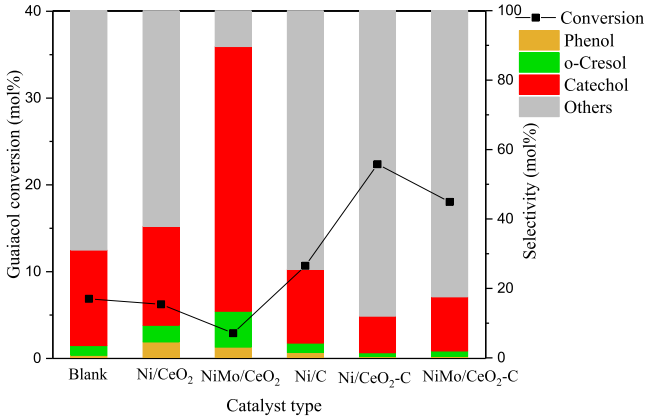


**Figure 4.** Activity of Ni-based catalysts in the water-only guaiacol HDO process.

$CeO_2$−C catalyst compared to 18% obtained for NiMo/$CeO_2$−C. Our results reflect the important role of C in the catalyst formulation because of multiple reasons. The AC support provides a high surface area, which is an essential feature to achieve high metallic dispersion.[42] Along with the excellent metallic dispersion, the strong metal-support interaction evidenced by TPR and the electronic contact intended from the XPS explains the enhanced activity of the $CeO_2$−C-supported catalysts. Moreover, the hydrophobicity and porosity of carbon aid to protect the active sites on the surface of catalysts against blockages with water and further facilitate the reactant to arrive at the active centers to realize the deoxygenation process. Indeed, water activation is as important as the activation of the organic molecules in this "$H_2$-free" HDO process because $H_2$ should come from water. Hence, in order to rule out the possible contribution of hydrogen released from the support (activated carbon) functional groups, a temperature-programmed desorption (TPD) analysis of the activated carbon was conducted (Figure S6). The result indicates that $H_2$ is only released from carbon functional groups when the temperature is higher than 800 °C. Because our process takes place at 250 °C, the contribution of hydrogen from the support is not plausible. Another potential pool of hydrogen is the organic molecule itself undergoing a reforming process. The investigation by Zhang et al. indicated that guaiacol will not undergo a steam-reforming process at temperatures under 300 °C.[43] Hence, we can discard this possibility for our particular process. Nevertheless, it is important to point out that the mono-aromatic products might be originated from the isomerization of guaiacol and the cracking of the side chains, and also the rearrangement of the functionalities of reactant as observed elsewhere.[43]

The selectivity toward partially de-oxygenated products is key to validate our approach. In general, three typical partial hydrogenated aromatic compounds were produced during the in situ HDO process, namely, phenol, *o*-cresol, and catechol. Other products (like benzene, 1,2-dimethoxy-; 4-nonanone; cyclopropane, octyl-; phenol, 2,4-bis(1,1 dimethylethyl); 1-undecene, 10-methyl; cyclopentane, 1,1,3-trimethyl; [1,1-biphenyl]-4,4-diol, 3-3-dimethoxy-, etc.) were also detected. The selectivity to these partial deoxygenated products plays a decisive role in the deoxygenation degree of the HDO process. The distribution of HDO products in Figure 4 shows that the selectivity toward partial deoxygenated products (catechol and *o*-cresol) was enhanced by the addition of Mo in the catalysts'


DOI: 10.1021/acssuschemeng.9b02712
ACS Sustainable Chem. Eng. 2019, 7, 16041−16049

formulation ($NiMo/CeO_2$ vs $Ni/CeO_2$; $NiMo/CeO_2$−C vs $Ni/CeO_2$−C). When comparing the activity/selectivity of the carbon-based materials it seems clear that the monometallic catalyst is slightly more active than the Ni−Mo system. Nevertheless, the Ni−Mo catalyst is more selective toward the desired products. Hence, it is inferred that the utilization of monometallic Ni leads in part also to a nonselective process in which the organic molecules are anchored to the catalyst either via the C−C or the C−O bonds (which may lead to multiple reactions such as cracking, polymerization, etc.). Interestingly, for the bimetallic catalysts, there is a preferential interaction with the C−O bond favoring the HDO route. The latter is ascribed to the Ni−Mo interaction which is reflected in the electronic surface composition discussed in the XPS section and also supported by the TPR results.

From the activity/selectivity data on Figure 4, it is not straightforward to establish a strong conclusion to select a "champion" catalyst. Therefore, we find it useful to report the deoxygenation ability of the catalyst in HDO ($X_{HDO}$ %, eq S3) (Figure S5) to compare the guaiacol conversion within the studied series, as reported elsewhere.[27] This HDO conversion can be used as a reference to evaluate the overall deoxygenation ability of a catalyst in which reactant conversion, product selectivity, and the amount of catalyst were taken into consideration. The $X_{HDO}$ % shows the same trend as guaiacol conversion. $X_{HDO}$ % over C-containing catalysts shows higher deoxygenation ability compared to $CeO_2$-supported catalysts. The slightly superior performance of $Ni/CeO_2$−C compared with $NiMo/CeO_2$−C is worth emphasizing, showing around 20 $X_{HDO}$ % compared to 15 $X_{HDO}$ %, respectively. It is clear that the addition of Mo improves the selectivity of the desired deoxygenated products, but in general terms (conversion/selectivity compromise), it seems that $Ni/CeO_2$−C is the best formulation.

A simplified representation of potential HDO pathways of guaiacol, based on the observed product distribution and previous work in literature, is presented in Figure 5.[44] Guaiacol can undergo a transalkylation process in which the methyl group on the methoxy group is transferred to the aromatic ring at the ortho position to produce methyl-catechol. Then, the two phenolic hydroxyls can be hydrogenolyzed to produce *o*-cresol. This pathway is favored in $CeO_2$-supported catalysts ($Ni/CeO_2$ and $NiMo/CeO_2$) considering the high ratio of *o*-cresol in the product distribution compared to that of $CeO_2$−C-supported catalysts ($Ni/CeO_2$−C and $NiMo/CeO_2$−C). The high selectivity to catechol in all the product distributions indicates the presence of other HDO pathways. The formation of catechol is the most preferred process because the C ($sp^3$)−O bond is most likely to be broken, as it presents the lowest bond energy.[44] As it has been discussed above, the addition of Mo favors this C−O cleavage, increasing the catechol selectivity in the Mo-containing samples. Guaiacol could undergo demethylation (DME) to produce catechol along with $CH_4$. Catechol can further produce partial deoxygenated products like phenol, through dehydroxylation (DHO) reaction. It is reported that catechol can easily undergo DHO to produce the complete deoxygenated product, phenol, during the HDO process with $H_2$ supply.[44] In contrast, the DHO reaction hardly happens in the water-only reaction system, which is a determinant step accounting for the relatively low deoxygenation ratio in the HDO processes. In practical terms, the enhancement toward the production of partially deoxygenated products is a breakthrough for the HDO reaction using water as hydrogen donor. For example, in the presence of $NiMo/CeO_2$, the selectivity of phenol and *o*-cresol is approximately four times compared to that of blank HDO reaction. Another possible pathway for the production of phenol is the direct demethoxylation (DMO) of guaiacol. The presence of this pathway can be judged by the traces of methanol in the product distribution. Anisole can be derived from the hydrogenation of C ($sp^2$)−OH bonds. Anisole can be further hydrodeoxygenated to phenol. The possibility of this route can be further speculated from the product distribution of short time HDO reaction because no anisole was detected in our HDO products after 4 h reaction.

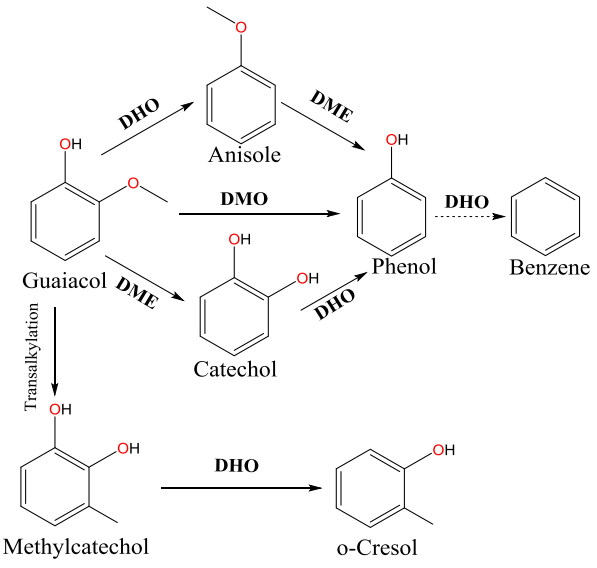


**Figure 5.** Proposed reaction pathways of guaiacol HDO over Ni-based catalysts (DMO; DME; DHO) (partially adopted from ref 44).

**Characterization of Spent Catalysts.** *X-ray diffraction.* Along with the catalysts' activity, the stability is a key parameter to consider for a realistic application. Given the relatively high pressures used in the process (50 bar) and the high concentration of organic carbon in the media, coking and sintering are the most likely deactivation phenomena. The carbon deposition of C-free catalysts and the sintering state of the active phases in all catalysts were studied by means of XRD analysis of spent catalysts. As shown in Figure 6, the typical peaks of metallic Ni at $2\theta$ = 44.5°, 51.8°, and 76.4° were detected in the spent catalysts[45] which are attributed to the reduction treatment of catalysts before the HDO reaction. The Ni clusters are small in all the samples, but smaller and highly dispersed in the C-based materials replicating the trend observed in the pre-activated solids. Indeed, for the C-based samples, it is hard to distinguish any crystalline reflection of metallic Ni, indicating the robustness of these materials toward sintering at high pressure. Also, it is important to highlight that Ni remains in its metallic state. As for the carbon deposition, the typical peaks, at $2\theta$ = 22° and 42°, which can be assigned to carbon, cannot be observed in the XRD pattern of spent $Ni/CeO_2$ and $NiMo/CeO_2$ catalysts, indicating the absence of major crystalline carbonaceous clusters in our materials after the HDO reaction.

*Transmission Electron Microscopy.* To further visualize the structural and morphological changes of C-containing catalysts, TEM micrographs of spent catalysts were taken to make a


DOI: 10.1021/acssuschemeng.9b02712
ACS Sustainable Chem. Eng. 2019, 7, 16041−16049

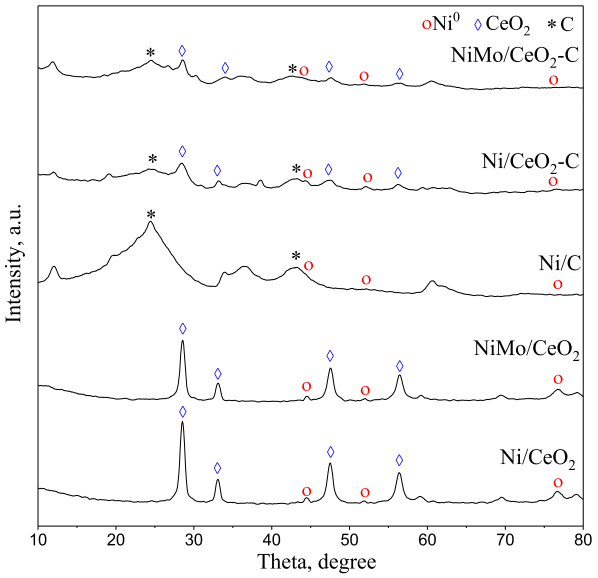


**Figure 6.** XRD patterns of spent catalysts.

comparison with the fresh ones (Figure 7). No carbon deposition or metal sintering was detected in the TEM images,

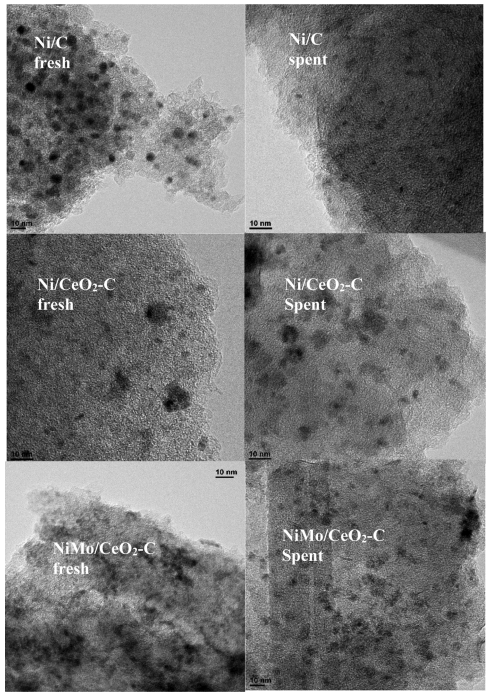


**Figure 7.** Selected TEM micrographs of fresh/spent C-containing catalysts.

in fair agreement with the XRD data, indicating the high stability of C-supported catalysts in the water reaction system. Indeed, the Ni−$CeO_2$ clusters remain well dispersed after the reaction.

For the sake of comparison, the TEM micrographs of the spent C-free catalysts are presented in the Supporting Information, showcasing also the stability of these materials during the reaction (Figure S7).

*Raman.* Raman spectroscopy is very sensitive to carbon and can reveal the presence of traces of carbonaceous species. Raman spectra of the spent C-free catalysts are presented in Figure 8. The typical bands centered at around 1340 $cm^{-1}$ (D band) and 1589 $cm^{-1}$ (G band), characteristic of carbon deposits, were observed. The G band is related to a graphitic carbon phase with an $sp^2$ electronic configuration, whereas the D band is a common feature of all disordered graphitic carbon.[46] The graphitization degree of carbon on the spent catalysts can be estimated from the relative intensity of these two bands ($I_G/I_D$).[47] The disordered graphitic structure is the main state of deposited carbon on the surface of spent catalysts, even though we could not observe it in the XRD diffractograms, the Ni/$CeO_2$ sample having a higher $I_G/I_D$ ratio. That means that Mo helps to avoid the graphitic carbon formation, emphasizing again its advantages as a promoter.

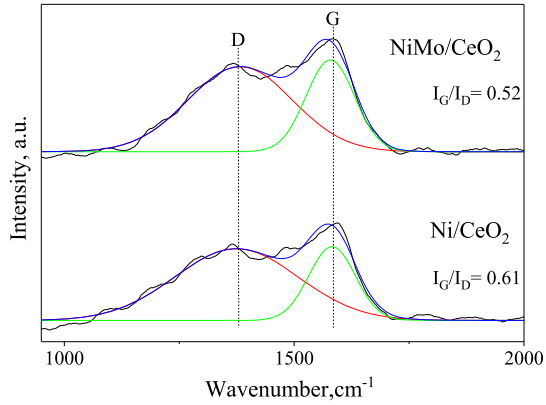


**Figure 8.** Raman spectra of spent $CeO_2$-supported catalysts.

## CONCLUSIONS

This work showcases a novel route for biomass upgrading via HDO reactions suppressing external hydrogen supply. We propose the use of water as a hydrogen donor and the utilization of multifunctional catalysts that are able to activate water and conduct the HDO. For a proof of concept, guaiacol was selected as a model compound to check the viability of this route using multicomponent Ni-based catalysts. We observed that Ni clusters doped with ceria and supported on a high surface area activated carbon are promising materials for this reaction, reaching conversion values beyond 20% under the studied conditions. Although such conversion values may look modest, it must be highlighted that the reaction only requires water (instead of hydrogen), which has a tremendous impact on the economic and safety aspects of the reaction. In addition, the selectivity toward partially de-oxygenated products is boosted by the presence of Mo, which retrieves electron density from Ni creating partial positive electronic charges on Ni clusters which are ideal to interact with the O−C bond in the biocompound.

The relatively high activity of $CeO_2$−C-supported catalysts can be attributed to the high dispersion of Ni nanoparticles on the support surface, the smaller particle size of ceria which leads to a higher Ni−$CeO_2$ interface, and also the abundance of oxygen vacancies existing in the support. Assuming that water activation happens on ceria oxygen vacancies, the O−C bond breaking is mediated by Ni clusters, and the subsequent reaction steps take place on the Ni−$CeO_2$ interface; the larger the interface, the greater is the activity. Therefore, dispersing ceria on carbon is a clever strategy to maximize the conversion


DOI: 10.1021/acssuschemeng.9b02712
ACS Sustainable Chem. Eng. 2019, 7, 16041−16049

in this reaction because smaller particle size of ceria particles is achieved leading to an extended Ni−$CeO_2$ interface and more chances for the reaction to successfully take place. Under these premises, and considering the product distribution, a reaction pathway can be proposed for the in situ HDO using water media where DHO of oxygenated aromatic compounds (e.g., phenol and catechol) plays a key role in the process. Nevertheless, further experiments are still needed to validate such a reaction pathway, which is beyond the scope of this proof-of-concept study. Very importantly, the developed catalysts do not show relevant means of deactivation by sintering and just traces of carbon deposits are observed, demonstrating their robustness in the studied reaction conditions.

Overall, although still preliminary, our hypothesis of "$H_2$-free" HDO reactions as potential economically advantageous route for biocompound upgrading seems to work for model molecules and opens further research avenues to optimize the catalysts and reactor design, as well as the operating conditions.

## ■ ASSOCIATED CONTENT

### Supporting Information

The Supporting Information is available free of charge on the ACS Publications website at DOI: 10.1021/acssuschemeng.9b02712.

Catalysts preparation methods; detailed description of the characterization techniques (XPS, Raman, XRD, $H_2$-TPR, $N_2$-adsorption and TEM); description of the reaction set-up and reaction conditions; XRD patterns of reduced catalysts; particle size distribution on the Ni/C catalyst; XPS spectra; HDO conversion data; TPD analysis; TEM images of the carbon-free catalysts after reaction (PDF)

## ■ AUTHOR INFORMATION


### Corresponding Author

*E-mail: t.ramirezreina@surrey.ac.uk.

### ORCID

S. Gu: 0000-0002-5675-9118

T. R. Reina: 0000-0001-9693-5107


### Notes

The authors declare no competing financial interest.

## ■ ACKNOWLEDGMENTS

Financial support for this work was provided by the Department of Chemical and Process Engineering of the University of Surrey and the EPSRC grants EP/J020184/2 and EP/R512904/1 as well as the Royal Society Research grant RSGR1180353. Authors would also like to acknowledge the Ministerio de Economía, Industrial Competitividad of Spain (project MAT2016-80285-P) and the Chinese Scholarship Council (CSC). L.P.-P. also thanks Comunitat Valenciana for her postdoctoral fellow APOSTD2017.

## ■ REFERENCES


(1) Lup, A. N. K.; Abnisa, F.; Daud, W. M. A. W.; Aroua, M. K. A review on reaction mechanisms of metal-catalyzed deoxygenation process in bio-oil model compounds. *Appl. Catal., A* **2017**, *541*, 87−106.

(2) Hoogwijk, M.; Faaij, A.; Van Den Broek, R.; Berndes, G.; Gielen, D.; Turkenburg, W. Exploration of the ranges of the global potential of biomass for energy. *Biomass Bioenergy* **2003**, *25*, 119−133.

(3) Field, C.; Campbell, J.; Lobell, D. Biomass energy: the scale of the potential resource. *Trends Ecol. Evol.* **2008**, *23*, 65−72.

(4) Furimsky, E. Catalytic hydrodeoxygenation. *Appl. Catal., A* **2000**, *199*, 147−190.

(5) Shi, Y.; Xing, E.; Wu, K.; Wang, J.; Yang, M.; Wu, Y. Recent progress on upgrading of bio-oil to hydrocarbons over metal/zeolite bifunctional catalysts. *Catal. Sci. Technol.* **2017**, *7*, 2385−2415.

(6) Wildschut, J.; Arentz, J.; Rasrendra, C. B.; Venderbosch, R. H.; Heeres, H. J. Catalytic hydrotreatment of fast pyrolysis oil: model studies on reaction pathways for the carbohydrate fraction. *Environ. Prog. Sustainable Energy* **2009**, *28*, 450−460.

(7) Robinson, A. M.; Hensley, J. E.; Medlin, J. W. Bifunctional catalysts for upgrading of biomass-derived oxygenates: A Review. *ACS Catal.* **2016**, *6*, 5026−5043.

(8) Elliott, D. C.; Wang, H.; Rover, M.; Whitmer, L.; Smith, R.; Brown, R. Hydrocarbon Liquid Production via Catalytic Hydroprocessing of Phenolic Oils Fractionated from Fast Pyrolysis of Red Oak and Corn Stover. *ACS Sustainable Chem. Eng.* **2015**, *3*, 892−902.

(9) Stiegel, G. J.; Ramezan, M. Hydrogen from coal gasification: An economical pathway to a sustainable energy future. *Int. J. Coal Geol.* **2006**, *65*, 173−190.

(10) Ursua, A.; Gandia, L. M.; Sanchis, P. Hydrogen production from water electrolysis: current status and future trends. *Proc. IEEE* **2012**, *100*, 410−426.

(11) Cohen, A.; Larsen, J. *Explosive Mechanism of the $H_2$−$O_2$ Reaction Near the Second Ignition Limit*; Ballistic Research Labs Aberdeen Proving Ground MD, 1967.

(12) Jin, W.; Pastor-Pérez, L.; Shen, D.; Sepúlveda-Escribano, A.; Gu, S.; Ramirez Reina, T. Catalytic upgrading of biomass model compounds: Novel approaches and lessons learnt from traditional hydrodeoxygenation-a review. *ChemCatChem* **2019**, *11*, 924−960.

(13) Nie, R.; Peng, X.; Zhang, H.; Yu, X.; Lu, X.; Zhou, D.; Xia, Q. Transfer hydrogenation of bio-fuel with formic acid over biomass-derived N-doped carbon supported acid-resistant Pd catalyst. *Catal. Sci. Technol.* **2017**, *7*, 627−634.

(14) Gilkey, M. J.; Xu, B. Heterogeneous Catalytic Transfer Hydrogenation as an Effective Pathway in Biomass Upgrading. *ACS Catal.* **2016**, *6*, 1420−1436.

(15) Xiao, Y.; Varma, A. Catalytic Deoxygenation of Guaiacol Using Methane. *ACS Sustainable Chem. Eng.* **2015**, *3*, 2606−2610.

(16) Wang, L.; Ye, P.; Yuan, F.; Li, S.; Ye, Z. Liquid phase in-situ hydrodeoxygenation of bio-derived phenol over Raney Ni and Nafion/$SiO_2$. *Int. J. Hydrogen Energy* **2015**, *40*, 14790−14797.

(17) Lee, J.-H.; Lee, I.-G.; Jeon, W.; Ha, J.-H.; Lee, K.-Y. Catalytic upgrading of bio-tar over a MgNiMo/activated charcoal catalyst under supercritical ethanol conditions. *Catal. Today* **2018**, *316*, 237−243.

(18) Lee, J.-H.; Lee, I.-G.; Park, J.-Y.; Lee, K.-Y. Efficient upgrading of pyrolysis bio-oil over Ni-based catalysts in supercritical ethanol. *Fuel* **2019**, *241*, 207−217.

(19) Cheng, S.; Wei, L.; Alsowij, M. R.; Corbin, F.; Julson, J.; Boakye, E.; Raynie, D. In situ hydrodeoxygenation upgrading of pine sawdust bio-oil to hydrocarbon biofuel using Pd/C catalyst. *J. Energy Inst.* **2018**, *91*, 163−171.

(20) Cheng, S.; Wei, L.; Julson, J.; Muthukumarappan, K.; Kharel, P. R.; Cao, Y.; Boakye, E.; Raynie, D.; Gu, Z. Hydrodeoxygenation upgrading of pine sawdust bio-oil using zinc metal with zero valency. *J. Taiwan Inst. Chem. Eng.* **2017**, *74*, 146−153.

(21) Rahimpour, M. R.; Jahanmiri, A.; Rostami, P.; Taghvaei, H.; Gates, B. C. Upgrading of Anisole in a Catalytic Pulsed Dielectric Barrier Discharge Plasma Reactor. *Energy Fuels* **2013**, *27*, 7424−7431.

(22) Taghvaei, H.; Hosseinzadeh, M. B.; Rezazadeh, S.; Rahimpour, M. R.; Shariati, A. Upgrading of 4-methylanisole in a catalytic reactor with electric discharges: A novel approach to O-removal from bio-oils. *Chem. Eng. J.* **2015**, *281*, 227−235.

(23) Mortensen, P. M.; Grunwaldt, J.-D.; Jensen, P. A.; Jensen, A. D. Influence on nickel particle size on the hydrodeoxygenation of phenol over Ni/SiO 2. *Catal. Today* **2016**, *259*, 277−284.
(24) Tran, C.-C.; Stankovikj, F.; Garcia-Perez, M.; Kaliaguine, S. Unsupported transition metal-catalyzed hydrodeoxygenation of guaiacol. *Catal. Commun.* **2017**, *101*, 71−76.
(25) Pastor-Pérez, L.; Buitrago-Sierra, R.; Sepúlveda-Escribano, A. $CeO_2$-promoted Ni/activated carbon catalysts for the water−gas shift (WGS) reaction. *Int. J. Hydrogen Energy* **2014**, *39*, 17589−17599.
(26) De, S.; Saha, B.; Luque, R. Hydrodeoxygenation processes: Advances on catalytic transformations of biomass-derived platform chemicals into hydrocarbon fuels. *Bioresour. Technol.* **2015**, *178*, 108−118.
(27) Olcese, R. N.; Bettahar, M.; Petitjean, D.; Malaman, B.; Giovanella, F.; Dufour, A. Gas-phase hydrodeoxygenation of guaiacol over Fe/$SiO_2$ catalyst. *Appl. Catal., B* **2012**, *115*−*116*, 63−73.
(28) Chayakul, K.; Srithanratana, T.; Hengrasmee, S. Catalytic activities of Re−Ni/CeO2 bimetallic catalysts for water gas shift reaction. *Catal. Today* **2011**, *175*, 420−429.
(29) Li, B.; Xu, X.; Zhang, S. Synthesis gas production in the combined CO2 reforming with partial;oxidation of methane over Ce-promoted Ni/$SiO_2$ catalysts. *Int. J. Hydrogen Energy* **2013**, *38*, 890−900.
(30) Phan, B. M. Q.; Ha, Q. L. M.; Le, N. P.; Ngo, P. T.; Nguyen, T. H.; Dang, T. T.; Nguyen, L. H.; Nguyen, D. A.; Luu, L. C. Influences of Various Supports, $\gamma$-$Al_2O_3$ , $CeO_2$ , and SBA-15 on HDO Performance of NiMo Catalyst. *Catal. Lett.* **2015**, *145*, 662−667.
(31) Myint, M. *Theoretical and Experimental Study of Bimetallic Catalysts in Heterogeneous Catalysis and Electrocatalysis for Energy Applications*; University of Delaware, 2015.
(32) le Saché, E.; Santos, J. L.; Smith, T. J.; Centeno, M. A.; Arellano-Garcia, H.; Odriozola, J. A.; Reina, T. R. Multicomponent Ni-CeO 2 nanocatalysts for syngas production from $CO_2$/$CH_4$ mixtures. *J. $CO_2$ Util.* **2018**, *25*, 68−78.
(33) García-Cerda, L. A.; Bernal-Ramos, K. M.; Montemayor, S. M.; Quevedo-López, M. A.; Betancourt-Galindo, R.; Bueno-Báques, D. Preparation of hcp and fcc Ni and Ni/NiO nanoparticles using a citric acid assisted pechini-type method. *J. Nanomater.* **2011**, *2011*, 162495.
(34) Serrano-Ruiz, J. C.; Ramos-Fernández, E. V.; Silvestre-Albero, J.; Sepúlveda-Escribano, A.; Rodríguez-Reinoso, F. Preparation and characterization of $CeO_2$ highly dispersed on activated carbon. *Mater. Res. Bull.* **2008**, *43*, 1850−1857.
(35) Shinde, V. M.; Madras, G. Nanostructured Pd modified Ni/$CeO_2$ catalyst for water gas shift and catalytic hydrogen combustion reaction. *Appl. Catal., B* **2013**, *132*−*133*, 28−38.
(36) Czekaj, I.; Loviat, F.; Raimondi, F.; Wambach, J.; Biollaz, S.; Wokaun, A. Characterization of surface processes at the Ni-based catalyst during the methanation of biomass-derived synthesis gas: X-ray photoelectron spectroscopy (XPS). *Appl. Catal., A* **2007**, *329*, 68−78.
(37) Senanayake, S. D.; Rodriguez, J. A.; Stacchiola, D. Electronic Metal−Support Interactions and the Production of Hydrogen Through the Water-Gas Shift Reaction and Ethanol Steam Reforming: Fundamental Studies with Well-Defined Model Catalysts. *Top. Catal.* **2013**, *56*, 1488−1498.
(38) Delporte, P.; Meunier, F.; Pham-Huu, C.; Vennegues, P.; Ledoux, M. J.; Guille, J. Physical characterization of molybdenum oxycarbide catalyst; TEM, XRD and XPS. *Catal. Today* **1995**, *23*, 251−267.
(39) Burroughs, P.; Hamnett, A.; Orchard, A. F.; Thornton, G. Satellite structure in the X-ray photoelectron spectra of some binary and mixed oxides of lanthanum and cerium. *J. Chem. Soc., Dalton Trans.* **1976**, 1686−1698.
(40) Boldrin, P.; Ruiz-Trejo, E.; Mermelstein, J.; Bermúdez Menéndez, J. M.; Ramírez Reina, T.; Brandon, N. P. Strategies for carbon and sulfur tolerant solid oxide fuel cell materials, incorporating lessons from heterogeneous catalysis. *Chem. Rev* **2016**, *116*, 13633−13684.
(41) Reina, T. R.; Ivanova, S.; Centeno, M. A.; Odriozola, J. A. Boosting the activity of a Au/$CeO_2$/$Al_2O_3$ catalyst for the WGS reaction. *Catal. Today* **2015**, *253*, 149−154.
(42) De, S.; Saha, B.; Luque, R. Hydrodeoxygenation processes: Advances on catalytic transformations of biomass-derived platform chemicals into hydrocarbon fuels. *Bioresour. Technol.* **2015**, *178*, 108−118.
(43) Zhang, Z.; Hu, X.; Zhang, L.; Yang, Y.; Li, Q.; Fan, H.; Liu, Q.; Wei, T.; Li, C.-Z. Steam reforming of guaiacol over Ni/$Al_2O_3$ and Ni/SBA-15: Impacts of support on catalytic behaviors of nickel and properties of coke. *Fuel Process. Technol.* **2019**, *191*, 138−151.
(44) Cai, Z.; Wang, F.; Zhang, X.; Ahishakiye, R.; Xie, Y.; Shen, Y. Selective hydrodeoxygenation of guaiacol to phenolics over activated carbon supported molybdenum catalysts. *Mol. Catal.* **2017**, *441*, 28−34.
(45) Kim, S. H.; Nam, S.-W.; Lim, T.-H.; Lee, H.-I. Effect of pretreatment on the activity of Ni catalyst for CO removal reaction by water−gas shift and methanation. *Appl. Catal., B* **2008**, *81*, 97−104.
(46) Ma, F.; Zhao, H.; Sun, L.; Li, Q.; Huo, L.; Xia, T.; Gao, S.; Pang, G.; Shi, Z.; Feng, S. A facile route for nitrogen-doped hollow graphitic carbon spheres with superior performance in super-capacitors. *J. Mater. Chem.* **2012**, *22*, 13464−13468.
(47) Zhang, J.; Wang, X.; Qi, G.; Li, B.; Song, Z.; Jiang, H.; Zhang, X.; Qiao, J. A novel N-doped porous carbon microsphere composed of hollow carbon nanospheres. *Carbon* **2016**, *96*, 864−870.


DOI: 10.1021/acssuschemeng.9b02712
*ACS Sustainable Chem. Eng.* 2019, 7, 16041−16049